A Study on Autonomous UAV Take-off and Landing on a Carrier

Somang Lee [1], Jihoon Lee [1], Seokwon Lee [1], Youdan Kim [1], Jinyoung Suk [2], and Seungkeun Kim [2]

[1] *Seoul National University, Seoul,* 08826, *Republic of Korea*
[2] *Chungnam National University, Daejeon,* 34134, *Republic of Korea*

Abstract

Landing on an aircraft carrier is one of the most challenging issues for Unmanned Aerial Vehicles (UAVs) because position and velocity of the landing site change as the aircraft carrier continuously moves on the sea. In addition, uncertain parameters such as winds and heights of the waves make the automatic landing/take-off problem more difficult. This study proposes an Automatic Carrier Landing System (ACLS) for UAVs including decision making process as well as guidance and control. The problem considered in this study is composed of three phases: take-off, approach, and landing. Suitable guidance and control laws are designed for each phase. Decision making logic is also developed based on the stochastic risk evaluation scheme. Numerical simulation results demonstrate the performance of the proposed decision making logic and guidance and control laws.

Keywords: Automatic carrier landing system, decision making, X-plane, UAV

I. Introduction

Automatic carrier landing is a challenging task for UAVs. There are several obstacles for the UAV to land on the carrier. First, the motion of the aircraft carrier should be estimated precisely. In contrast with a normal automatic landing on the ground, the landing site on the carrier wavers as the carrier moves on the sea. Also, the attitude of the aircraft carrier should be considered for the landing. The heave motion of the ship is especially critical in the aircraft carrier landing because only a small variation of the pitch angle of the carrier causes the landing site to change considerably in vertical direction. In addition, the fickle changes of sea state and gust make it difficult for landing on the carrier. Moreover, burble effect occurring in the region of turbulent air flow due to the air wake of the carrier should be considered [1]. It may cause the UAV to fail to land on the carrier because of the loss of lift due to the sharply decreased speed in the region. The narrow landing area of the aircraft carrier is also a harsh constraint of the automatic carrier landing.

For many years, automatic carrier landing has been studied. The robust controller for F/A-18A automatic carrier landing was proposed using finite horizon H-infinity techniques [2]. Steinberg et al. designed several controllers using neural net, fuzzy, evolutionary, and adaptive approaches for carrier landing [3]. An altitude controller was proposed for the final stage of aircraft carrier landing using LMI-based robust control theory [4]. A robust ACLS based on nonlinear dynamic inversion was proposed, and the ACLS was simulated and assessed for several cases [5]. Zhu et al. developed approach power compensation system which was a part of ACLS in order to improve tracking performance using conditional integral sliding surface [6]. Meanwhile, risk evaluation for decision making at the final landing phase has been widely studied [7-9]. Most studies, however, concentrated on a specific problem rather than the whole operation of UAVs.

In this study, ACLS including guidance, control, and decision making is considered for a whole scenario. For this purpose, the system is constructed based on MATLAB/Simulink and X-plane which is a well-known aircraft simulation software having reliable aerodynamics and aircraft models. Several recent works adopted this aircraft simulation software to verify their control and guidance algorithm [10, 11]. In this study, the ACLS simulates the whole scenario including autonomous take-off, approaching, and landing on an aircraft carrier via X-Plane. Decision making logic is also included in the ACLS to avoid the collision between a UAV and an aircraft carrier.

This paper is organized as follows. Section II describes the structure and components of the ACLS. Control and guidance law, and decision making logic are given in section II. In section III, numerical simulations are conducted to demonstrate the performance of the proposed scheme. Conclusion of this study is summarized in section IV.

II. Automatic Carrier Landing System

Simulation Scenario

Figure 1 shows the scenario considered in this study. The scenario is composed of three successive phases. The first phase is a take-off phase. A UAV is placed on a shot position of an aircraft carrier at first, and the UAV is launched using catapult. After the launch, by the catapult, the UAV takes off automatically by the take-off controller. When it reaches the desired altitude, the UAV moves to the next phase, i.e., an approach phase. At the approach phase, the UAV passes through designated waypoints. Six waypoints are selected to generate the trajectory of the UAV, thereby the UAV approaches the landing marshal point. After the approach phase, the UAV enters a landing phase where the UAV descends along the specific glide slope by the landing guidance law. Decision making process determines whether the UAV should continue landing in the landing phase or not. If the probability of failure such as bolter and collision is expected to be high, then the UAV waves off to retry the landing procedure. The details of each phase are given below. The guidance and control laws are designed mainly based on Ref. [12].

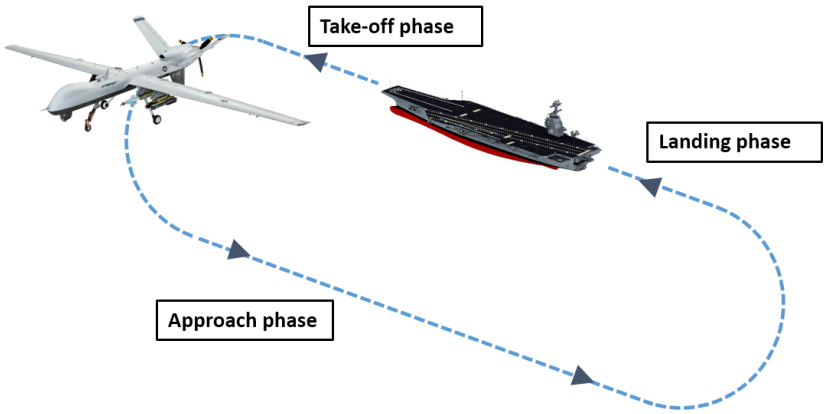


Fig. 1: The three phases of simulation scenario

i) Take-off Phase

A manned aircraft usually takes off on an aircraft carrier using full throttle and fixed elevator command. If the aircraft reaches a specific altitude, then the pilot manually controls the aircraft. In this study, the proposed ACLS of the UAV mimics this two-step approach.

At step 1, the throttle and elevator commands are fixed as 1 and 0.55, respectively. Note that the throttle command is normalized between $[0,1]$, and the control surfaces including elevator, rudder, and aileron are normalized between $[-1,1]$. In contrast with the longitudinal motion, the lateral motion is controlled to maintain $\phi_c = 0$ using Linear Quadratic Tracker (LQT) [12].

The UAV performs the next step when its altitude reaches 500 ft. In step 2, the lateral controller is same as in that of step 1, whereas the longitudinal controller is different. Rather than fixed control surface commands, elevator and throttle commands are generated to follow the constant flight path angle $\gamma_c = 5\text{deg}$ by Linear Quadratic Regulator (LQR) with the augmentation of integral error variable $s_\gamma = \int (\gamma - \gamma_c) dt$ [12].

ii) Approach Phase

Sometimes, an aircraft conducts a special mission such as reconnaissance or surveillance. In this study, the mission of the UAV is to approach the marshal point for landing. When the UAV's altitude reaches 820 ft, it moves to the approach phase. In this phase, the UAV passes through six waypoints. The waypoints are generated based on the position of the UAV when the UAV enters the approach phase. For waypoint guidance, the heading angle and flight path angle commands are obtained using the geometric relation between the waypoint and the current UAV position. Let us denote the positions of the waypoint and UAV, p_{way} and p_{uav}, as follows.

$$p_{way} = \begin{bmatrix} x_{way} & y_{way} & z_{way} \end{bmatrix}^T \tag{1}$$

$$p_{uav} = \begin{bmatrix} x_{uav} & y_{uav} & z_{uav} \end{bmatrix}^T \tag{2}$$

Then, χ_c and γ_c can be obtained as

$$\chi_c = \tan^{-1}\left(\frac{y_{way} - y_{uav}}{x_{way} - x_{uav}}\right) \tag{3}$$

$$\gamma_c = \tan^{-1}\left(\frac{-\left(z_{way} - z_{uav}\right)}{x_{way} - z_{uav}}\right) \tag{4}$$

The controller designed for the take-off phase is used in the approach and landing phases. The longitudinal and lateral autopilots make the UAV follow the generated χ_c and γ_c commands. Here, the χ_c command is converted to ϕ_c command using the following relation because ϕ_c is the state variable of the lateral linear model.

$$\phi_c = \tan^{-1}\left(\frac{V_c \dot{\chi}_c}{g\cos\theta}\right) \tag{5}$$

iii) Landing Phase

After passing through all waypoints, the UAV enters the landing phase. The outputs of this guidance law are heading angle command χ_c and flight path angle command γ_c. Let us define angles λ and η as in Fig. 2.

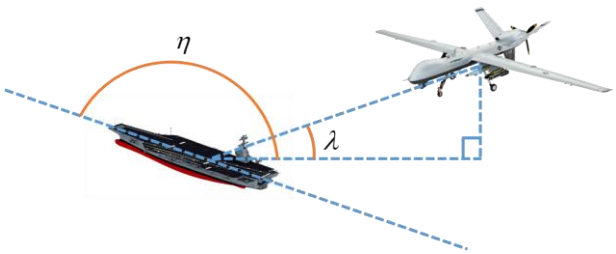


Fig. 2: The definition of angles λ and η

Let us also define $\begin{bmatrix}\bar{u} & \bar{v} & \bar{w}\end{bmatrix}^T$ as follows

$$\begin{bmatrix}\bar{u}\\ \bar{v}\\ \bar{w}\end{bmatrix} = V_s + \dot{\eta}\begin{bmatrix}-d\cos\lambda\sin\eta\\ d\cos\lambda\cos\eta\\ 0\end{bmatrix} + \dot{\lambda}\begin{bmatrix}-d\sin\lambda\cos\eta\\ -d\sin\lambda\sin\eta\\ -d\cos\lambda\end{bmatrix} \tag{6}$$

where V_s is the velocity of an aircraft carrier and V_{ref} is the reference velocity of the UAV. Then, $\dot{d}$ can be obtained by solving the following equation.

$$\dot{d}^2 + 2\left(\bar{u}\cos\lambda\cos\eta + \bar{v}\cos\lambda\sin\eta - \bar{w}\sin\lambda\right)\dot{d} + \left(\bar{u}^2 + \bar{v}^2 + \bar{w}^2\right) - {V_{ref}}^2 = 0 \tag{7}$$

Finally, the guidance commands can be obtained as follows.

$$\chi_c = \tan^{-1}\left(\frac{\bar{v} + \dot{d}\cos\lambda\sin\eta}{\bar{u} + \dot{d}\cos\lambda\cos\eta}\right) \tag{8}$$

$$\gamma_c = \sin^{-1}\left(\frac{-\left(\bar{w} - \dot{d}\sin\lambda\right)}{V_{ref}}\right) \tag{9}$$

LQR controller with integral error variable for the longitudinal motion and LQT for the lateral motion are used in the landing phase to track the guidance output.

Guidance laws and control laws used in each phase are summarized in Table 1.

Table 1: Guidance and control law for each phase

Phase		*Guidance law*	*Control law*
Take-off	Step 1	Longitudinal: Unnecessary Lateral: $\phi_c = 0$	Longitudinal: $\delta_T = 1$, $\delta_e = 0.55$ Lateral: LQT
	Step 2	Longitudinal: $\gamma_c = 5\text{deg}$ Lateral: $\phi_c = 0$	Longitudinal: LQR with integral error variable Lateral: LQT
Approach		Waypoint guidance based on geometric relation γ_c, χ_c	
Landing		Terminal guidance law γ_c, χ_c	

Decision Making

Decision Making block determines whether the UAV goes to the next step or not. In the ACLS, the autonomous take-off and landing scenario is composed of several steps based on the standard for manned aircraft of U.S. Navy [13]. Figure 3 shows the steps of the whole scenario. There are take-off and approach phases as mentioned in the previous section. Landing phase, however, is divided into several steps because a precise decision making is required in the landing phase. Sub-steps of landing phase are shown as blue boxes in Fig. 3.

Descent step means that the UAV is descending. In freeze step, all control commands are fixed for 1.5 seconds to prevent sharp maneuver. Touch down step means that the UAV touches the aircraft carrier, and engaged step is that the hook is arrested normally. During these steps, the decision making block evaluates the risk of the autonomous landing in real-time. If the estimated risk exceeds the threshold value during the descent step, the UAV enters the wave-off phase and performs wave-off maneuver using the take-off controller. Similarly, during the touch down step, the UAV may move to bolter step. The UAV finally arrives at recovered step if landing is successful or at failure step if not.

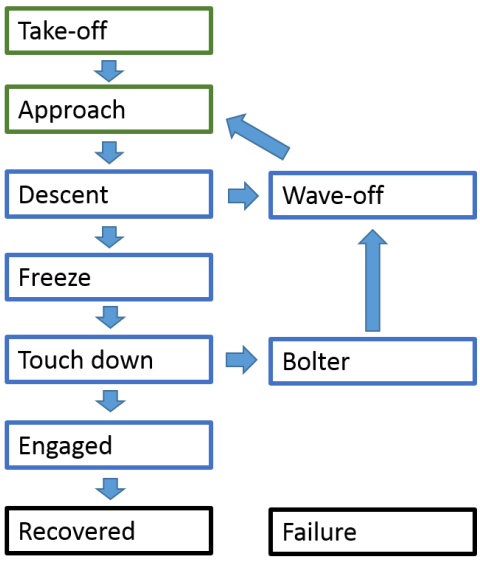


Fig. 3: The flow chart of decision making block

To determine the degree of risk, the decision making process based on a probabilistic approach is designed. Assuming that the errors have Gaussian distribution, the risk of failure can be estimated. In Fig. 4, the error variables used in risk estimation is shown. The errors related to roll angle, pitch angle, sideway velocity, vertical position, horizontal position, and sink rate are utilized to determine the degree of risk. Stateflow, the function of Simulink, is used to implement the decision making procedure in the ACLS. The implemented decision making block is shown in Fig. 5.

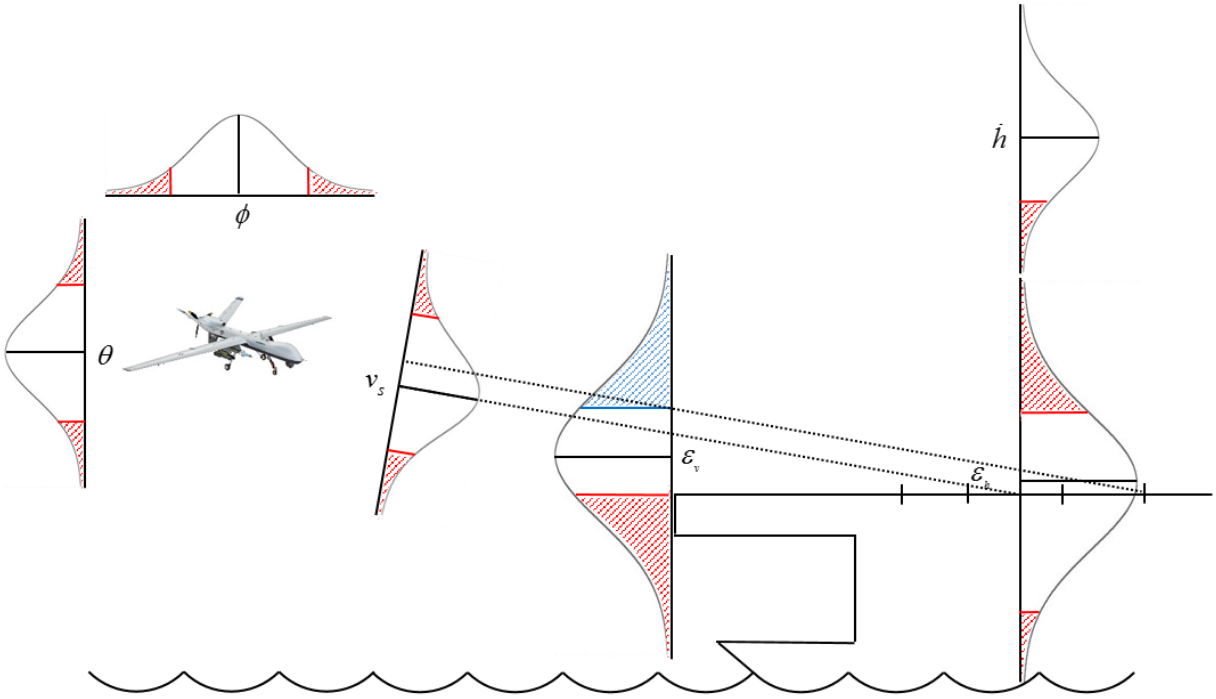


Fig. 4: The error variables used in risk estimation

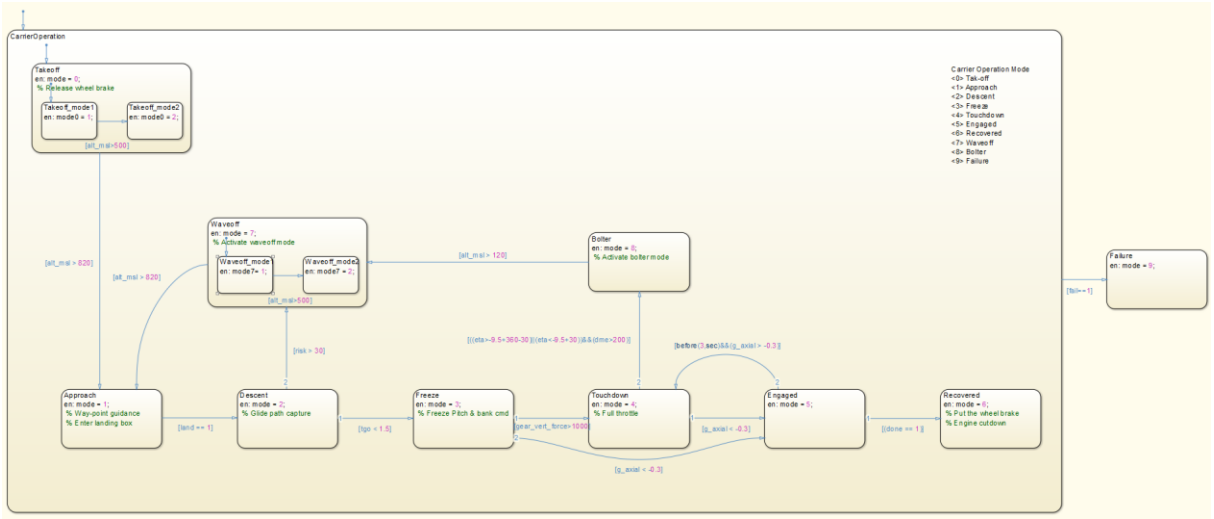


Fig. 5: Stateflow function of decision making block

ACLS Simulator

Figure 6 shows the block diagram of the simulator. The first block is a sensor block which receives data from X-plane through UDP network. With these data, guidance block generates guidance commands, and controller block computes the required control commands to follow the guidance commands. Actuator block passes the control commands and other information to X-plane via UDP network. Decision making block is located at the top of Fig. 6.

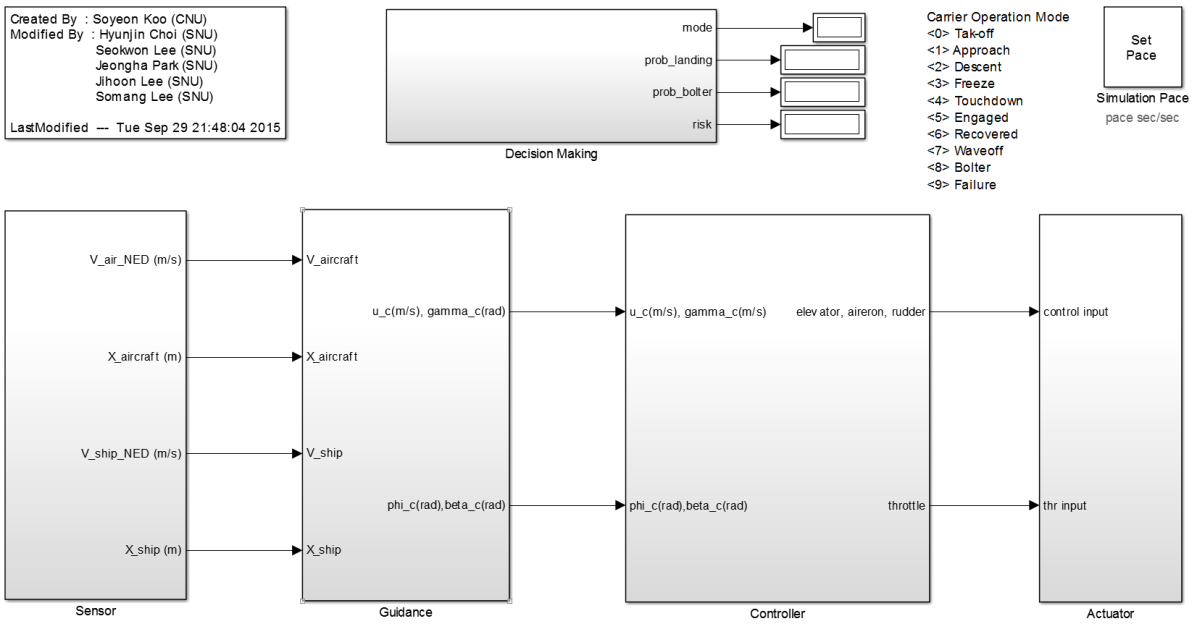


Fig. 6: The block diagram of the simulator

III. Simulation Results

Numerical simulation is conducted with the simulator and the scenario presented in section II. MQ-9 reaper is chosen as a reference UAV and Nimitz class as an aircraft carrier. Figure 7 shows the screenshot of X-plane software while the simulation is conducted.

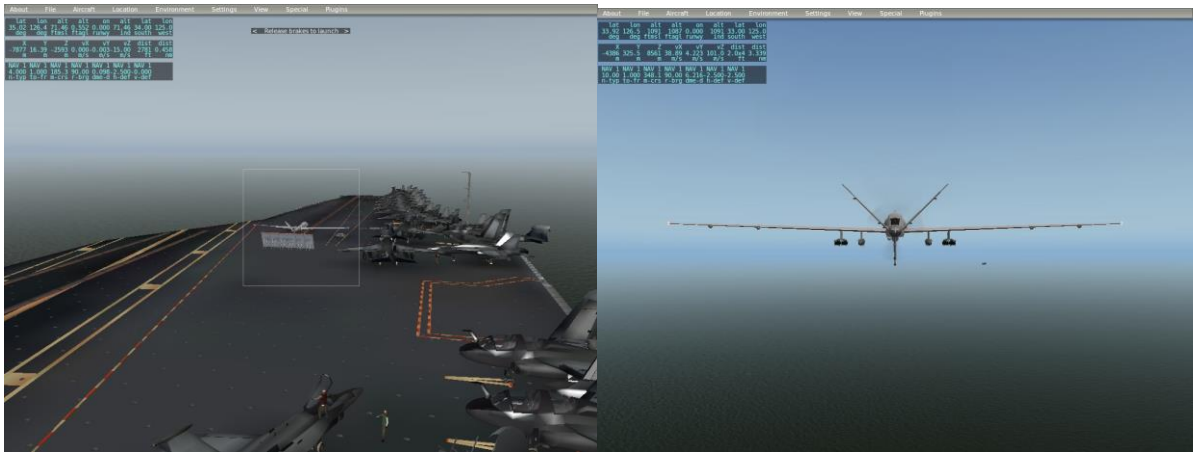


Fig. 7: Numerical simulation on X-Plane

Figure 8 shows the trajectory of the UAV and the aircraft carrier for a success case. Waypoints are represented as pink mark. Blue line denotes the trajectory of the UAV, and black line denotes the trajectory of the aircraft carrier. The ground path of the UAV is shown in red line. As shown in Fig. 8, the UAV takes off autonomously and approaches the rear part of the aircraft carrier in counter clockwise direction after visiting the waypoints successfully. After passing through all waypoints, the UAV descends to the aircraft carrier along the reference glide path.

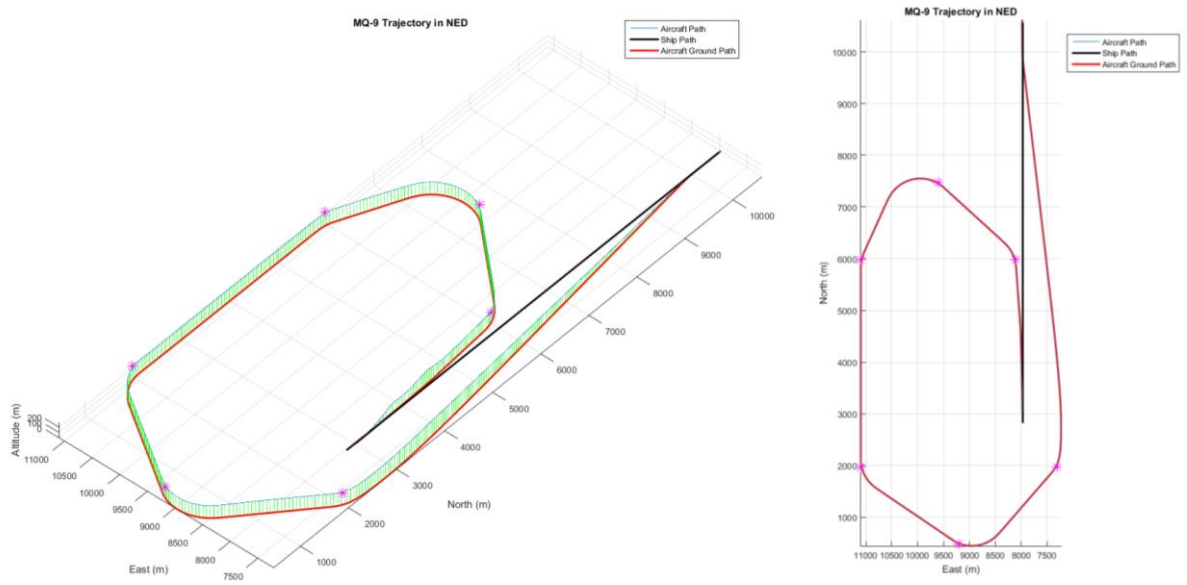


Fig. 8: Trajectory of UAV and aircraft carrier for a success case

Guidance commands and actual responses are shown in Fig. 9. As shown in Fig. 9, the state response of the UAV tracks the guidance command properly by the proposed controller. Note that jump discontinuity exists in heading angle command due to the drastic change of guidance command caused by the switch of phases or waypoints.
Control input responses are shown in Fig. 10. In lateral inputs, the large rudder input is used during the approach phase because the UAV has weak rudder power. During the other phases, the lateral inputs are rarely used for the maneuver of the UAV. The longitudinal control inputs, throttle and elevator, have quite different behavior. A chattering phenomenon is observed in throttle command especially at take-off phase, and elevator command does varies slightly. This difference results from that the longitudinal and lateral controllers are designed separately.

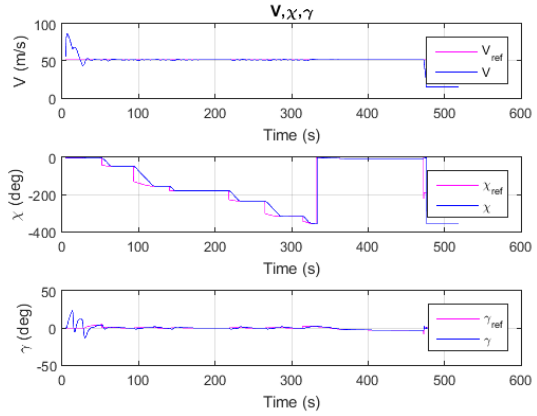


Fig. 9: Guidance commands and actual responses

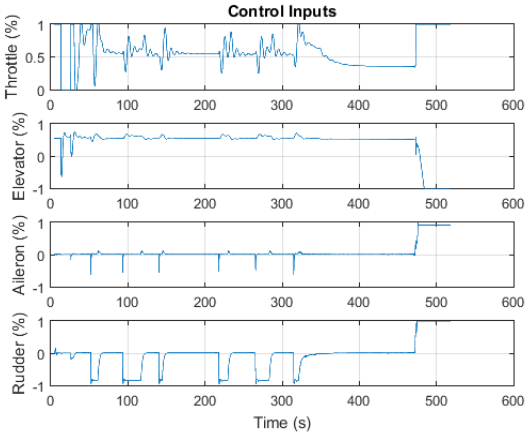


Fig. 10: Control input responses

Figures 11 and 12 show the results of decision making during the simulation for recovery and wave-off cases at the landing phase. The probability of successful landing is shown in the first row, and the probability of bolter is shown in the second row. The third row shows the overall risk during the simulation. Under Gaussian assumption, these probabilities are estimated using several variables including the position, velocity and attitude. Note that the decision making block is enabled only for 40 seconds. before touch down. In Fig. 11, the probability of landing is one and the probability of bolter is zero for the whole landing phase. Finally, the decision making block of the simulator concludes that the UAV can land on the aircraft carrier successfully. Based on the probabilities of successful landing and bolter, the estimated risk determines whether the UAV performs the wave-off maneuver at the landing phase or not. The third row of Fig. 11 indicates that the wave-off maneuver is unnecessary for recovery case because the threshold value of the risk for wave-off is set to 0.25. In contrast with Fig.11, Fig. 12 shows a different tendency. To simulate the wave-off case, the strong wind disturbance is exerted to the UAV. After 500 seconds, the decision making block estimates that the degree of risk is over 0.5, and thereby the UAV performs the wave-off maneuver. Therefore, Figs.11 and 12 verify the adequacy of the decision making process.

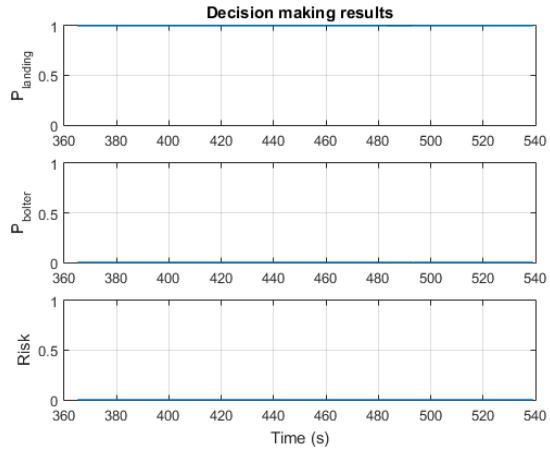


Fig. 11: Decision making results for recovery case

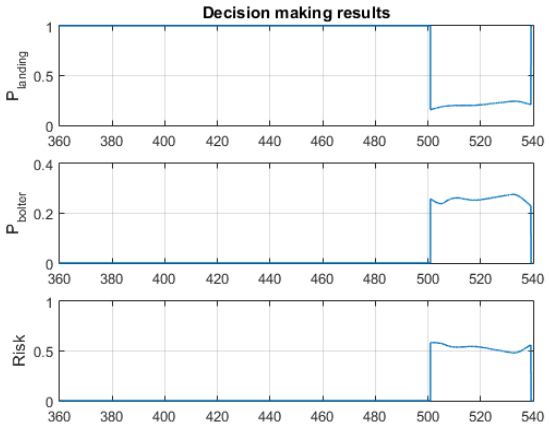


Fig. 12: Decision making results for wave-off case

IV. Conclusion

The whole operation of the autonomous carrier landing system was considered in this study. The proposed ACLS considers the scenario including three phases: take-off, approach, and landing phase. For each phase, appropriate guidance law and controller were designed to perform the specified mission. Decision making logic was also included in the system to avoid failure during the landing procedure. The ACLS was constructed on MATLAB/Simulink platform, and X-plane software was adopted to construct a trust-worthy feasible simulator in the sense of aerodynamics. Numerical simulation results demonstrated that the proposed control and guidance laws as well as the decision making logic are successful. Further studies such as a disturbance robust controller at the landing phase will be done using this simulator.

V. Acknowledgments

This work is supported by the Agency for Defense Development, Republic of Korea, under the Grant UD1130053JD.

References

1 Cherry, B.E., and Constantino, M.M., "The Burble Effect: Superstructure and Flight Deck Effects on Carrier Air Wake," *Proceedings of American Society of Naval Engineers Launch & Recovery Symposium 2010*, Arlington, VA, December 8-9, 2010.

2 Subrahmanyam, M.B., "H-infinity Design of F/A-18A Automatic Carrier Landing System," *Journal of Guidance, Control, and Dynamics*, Vol. 17, No. 1, 1994, pp. 187-191.

3 Steinberg, M., and Page, A., "A Comparison of Neural, Fuzzy, Evolutionary, and Adaptive Approaches for Carrier Landing," *AIAA Guidance, Navigation, and Control Conference*, Montreal, Canada, August 6-9, 2001.

4 Zhang, Y., Yang, Y., and Yu, Y., "Integrated Flight Thrust Control via LMI-Based H-infinity Synthesis in Automatic Carrier Landing System," *International Conference on Computational Intelligence for Modelling, Control and Automation, and International Conference on Intelligent Agents, Web Technologies and Internet Commerce*, Vienna, Austria, November 28-30, 2005.

5 Denison, N.A., Automated Carrier Landing of an Unmanned Combat Aerial Vehicle Using Dynamic Inversion, MS Thesis, Department of the Air Force Air University, Air Force Institute of Technology Wright-Patterson Air Force Base, OH, 2007.

6 Zhu, Q., Yu, Y., Zhang, Z., Zhang, W., and Wen, Z., "Design of Approach Power Compensation System for Carrier-Based Aircraft Using Conditional Integral Sliding Surface," *IEEE International Conference on Information and Automation*, Shenyang, China, June 6-8, 2012, pp. 821-826.

7. Johnstone, R.B., “Development of the Waveoff Decision Device,” *Journal of Aircraft*, Vol. 6, No. 4, 1969, pp. 367–371.

8. Jiang, H.T., Su, X.D., and Li, H., “Ramp-Strike Risk Evaluation Making of Carrier-Based Aircraft,” *International Journal of Control and Automation*, Vol. 7, No. 10, 2014, pp. 321–330.

9. Durand, T.S., and Wasicko, R.J., “Factors Influencing Glide Path Control in Carrier Landing,” *Journal of Aircraft*, Vol. 4, No. 2, 1967, pp. 146–158.

10 Santos, S.R.B. dos, Júnior, C.L.N., Junior, S.N.G., Bittar, A., and Oliveira, N.M.F. de, "Experimental Framework for Evaluation of Guidance and Control Algorithms for UAVs," *21st Brazilian Congress of Mechanical Engineering*, Natal, RN, Brazil, October 24-28, 2011.

11 Bittar, A., Figuereido, H.V., Guimaraes, P.A., and Mendes, A.C., "Guidance Software-In-the-Loop Simulation Using X-Plane and Simulink for UAVs," *International Conference on Unmanned Aircraft Systems*, Orlando, FL, May 27-30, 2014, pp. 993-1002.

12 Lee, S., Choi, H., Kim, Y., Kim, S., Kim, S., and Suk, J., “Unmanned Aerial Vehicles Glide-Path-Angle-Tracking for Autonomous Carrier Landing,” *Asia-Pacific International Symposium on Aerospace Technology*, Shanghai, China, September 24-26, 2014.

13 U.S. Navy, Aviation Electronics Technician 1 (Organizational), NAVEDTRA 14030, 1993.